Quantum Electronics **50** (4) 343–349 (2020)

https://doi.org/10.1070/QEL17311

Generation of few-cycle pulses in media with alternating sign of effective cubic nonlinearity

S.A. Frolov, V.I. Trunov, S.N. Bagayev

Abstract. **An original technique is developed for spectral broadening of femtosecond pulses with compensation for the nonlinear spatial phase during the propagation through nonlinear media with effective cubic nonlinearity of different signs. It was shown that in the region of 1.5 μm, the proposed scheme with BBO crystals at the first stage and NaCl at the second stage allows, using chirped mirrors, the formation of few-cycle pulses of about 7 fs duration with a small *B*-integral. The possibility of focusing of pulses compressed in the proposed scheme with a large Strehl ratio is demonstrated.**

Keywords: *few-cycle pulses, nonlinear compression, cubic nonlinearity, negative cascaded quadratic nonlinearity, multi-element spectral broadening, Strehl ratio.*

1. Introduction

Currently, work is underway to develop methods for increasing the peak power of radiation pulses of existing and designed petawatt and multipetawatt laser systems by spectral broadening in nonlinear optical crystals [1] and in optical solid materials with Kerr cubic nonlinearity [2–4], followed by compression of pulses with chirped mirrors.

More than 50-fold compression of millijoule pulses (from 170 to 3.2 fs) as they passed through a sequence of quartz plates was experimentally demonstrated [5]. In a similar scheme for femtosecond pulses of a microjoule level with phase stabilisation between the carrier and envelope, compression from 7 to 3.9 fs [6] and generation of pulses close to single-cycle ones (with a pulse shortened from 5.5 to 2.5 fs) [7] were experimentally demonstrated. The possibility of pulse shortening from 180 to 30 fs by spectral broadening using negative cascaded quadratic nonlinearity was also demonstrated [8]. The main difficulty in generating reproducible high-power spectrally broadened femtosecond pulses and their subsequent compression to a few optical cycles is related to a high level of the arising spatially inhomogeneous spectral phase caused by the Kerr cubic nonlinearity [9]. Nevertheless, using spatial filtering methods, 2–3-fold compression of pulses with an energy of up to 12 J to a duration of ~20 fs during propagation through media with cubic nonlinearity is currently experimentally implemented [10, 11]. An important factor characterising the quality of compressed pulses is their focusability. In Ref. [12], when focusing pulses compressed by less than two times, with energies of about 2 J and an initial duration of 55 fs, a decrease in the fraction of energy localised in the central spot, i.e., a decrease in the Strehl ratio, was experimentally observed.

In this paper, we present and study the scheme of pulse compression in time by phase self-modulation in nonlinear media with alternating sign of effective cubic nonlinearity. The scheme involves a stage with negative quadratic nonlinearity, followed by a stage with positive Kerr cubic nonlinearity. The length of the first medium is chosen such as to maximise spectral broadening, and the second one to provide optimal compensation of the nonlinear phase incursion. This approach allows significant reduction of the residual nonlinear spatial phase in comparison with multi-element spectral broadening schemes based on media with positive cubic nonlinearity [13]. Since optically transparent solid-state media with negative Kerr cubic nonlinearity are not known, cascaded quadratic nonlinearity is the only way to implement it.

S.A. Frolov, S.N. Bagayev Institute of Laser Physics, Siberian Branch, Russian Academy of Sciences, prosp. Akad. Lavrent'eva 13/3, 630090 Novosibirsk, Russia; e-mail: stanislav.a.frolov@gmail.com;
V.I. Trunov Institute of Laser Physics, Siberian Branch, Russian Academy of Sciences, prosp. Akad. Lavrent'eva 13/3, 630090 Novosibirsk, Russia; Novosibirsk State University, ul. Pirogova 2, 630090 Novosibirsk, Russia

Received 4 March 2020
Kvantovaya Elektronika **50** (4) 343–349 (2020)
Translated by V.L. Derbov

2. Negative cascaded quadratic nonlinearity in crystals with quadratic nonlinearity

2.1. Analytical formulae for effective cubic nonlinearity

The most common approach to describing the nonlinear phase caused by SHG in crystals with quadratic nonlinearity is to consider it as the phase induced by the effective cubic nonlinearity $n_{2,\mathrm{casc}}$, the magnitude of which depends on the wave mismatch Δk and the corresponding coefficient of quadratic nonlinearity [14]:

$$n_{2,\mathrm{casc}} = \frac{4\pi d_{\mathrm{eff}}^2}{\varepsilon_0 c\lambda n^3 \Delta k}, \tag{1}$$

where Δk is the wave mismatch for SHG of the first type; d_{eff} is the effective coefficient of quadratic nonlinearity; λ is the centre wavelength; and ε_0 is the electric constant.

A more accurate formula for calculating the nonlinear cascade phase is presented in Ref. [15]; it is valid for conversion efficiency up to 30%:

$$n_{2,\mathrm{casc}} = \frac{\pi\Delta k d_{\mathrm{eff}}^2}{\varepsilon_0 c\lambda n^3 Q^2}\left[1 - \frac{\sin(QL)}{2QL}\right], \tag{2}$$

where $Q = \sqrt{2\sigma^2 E^2 + \Delta k^2/4}$; E is the electric field; L is the length of the crystal; and $\sigma = 2\pi d_{\mathrm{eff}}/(\lambda n)$. From the presented formulae, it follows that, in comparison with the Kerr cubic nonlinearity, the effective coefficient of cascaded quadratic

nonlinearity sharply depends on the wavelength in accordance with the dependence of the wave mismatch. Moreover, with increasing conversion efficiency ($\sigma E \sim \Delta k$), a dependence on the intensity appears, i.e., the nonlinearity ceases to be cubic, and for $\sigma E \gg \Delta k$ the nonlinearity tends to zero with increasing intensity.

As follows from the above formulae, the sign of effective nonlinearity corresponds to the sign of the wave mismatch, and the maximum nonlinearity is achieved at a small nonzero wave mismatch. Approximately, the wave mismatch for maximum nonlinearity can be found from Eqn (2), which also implies the dependence of nonlinearity on intensity: as the intensity increases, the nonlinearity decreases.

2.2. Calculation of the spectral-angular distributions of the effective cubic nonlinearity

Using formulae (1) and (2), the spectral-angular distributions of the effective cubic nonlinearity were studied in various crystals. As follows from these formulae, to achieve a larger value of effective nonlinearity, a larger value of the coefficient d_{eff} is needed. The BBO crystal was chosen because of its high quadratic nonlinearity ($d_{\text{eff}} = 2.1$ pm V^{-1} at a phase-matching angle of 23° for the interaction of the first type). The LBO (XY plane), YCOB (XZ plane), and DKDP crystals were chosen because of their large available aperture, and the corresponding biaxial crystal planes were such that the quadratic nonlinearity was maximum. Figure 1 shows the spectral-angular distributions of $n_{2,\text{casc}}$ calculated using Eqn (2). As noted above, there are regions of positive and negative nonlinearities, in accordance with the wave mismatch sign. From the distributions shown in Fig. 1, it is seen that the spectral dispersion of cascaded nonlinearity is significant. Nevertheless, there are spectral regions in which this dispersion decreases to zero. These are regions where the group velocities of the waves of the first and the second harmonic coincide, i.e., the derivative of the wave mismatch with respect to wavelength is equal to zero. In the XY plane of LBO crystal, such a region is absent, while it exists in other planes, however, the value of the quadratic, and hence the cascaded quadratic nonlinearity is much smaller.

Spectral dependences of the total effective nonlinearity, i.e., the sum of the effective and Kerr (n_2) cubic nonlinearities for BBO and YCOB crystals at the propagation angles indicated in Fig. 1, are presented in Fig. 2 (for BBO $n_2 = 5.7 \times 10^{-16}$ cm^2 W^{-1}, and for YCOB $n_2 = 7.5 \times 10^{-16}$ cm^2 W^{-1}). The choice of these crystals is justified by their negative total effective cubic nonlinearity; this allows realising the nonlinear phase compensation at the second stage. We considered two values of the propagation angle, which allowed implementing effective cubic nonlinearity in the wavelength region near 0.83 μm, as well as in the spectral regions where the group wave velocities of the first and second harmonics coincide. For BBO, it is 1.55 μm, for YCOB – 1.6 μm. Figure 2 shows the results of calculations performed using both Eqn (1) corresponding to the approximation of low-efficiency conversion (low intensity or large wave mismatch), and Eqn (2) valid for

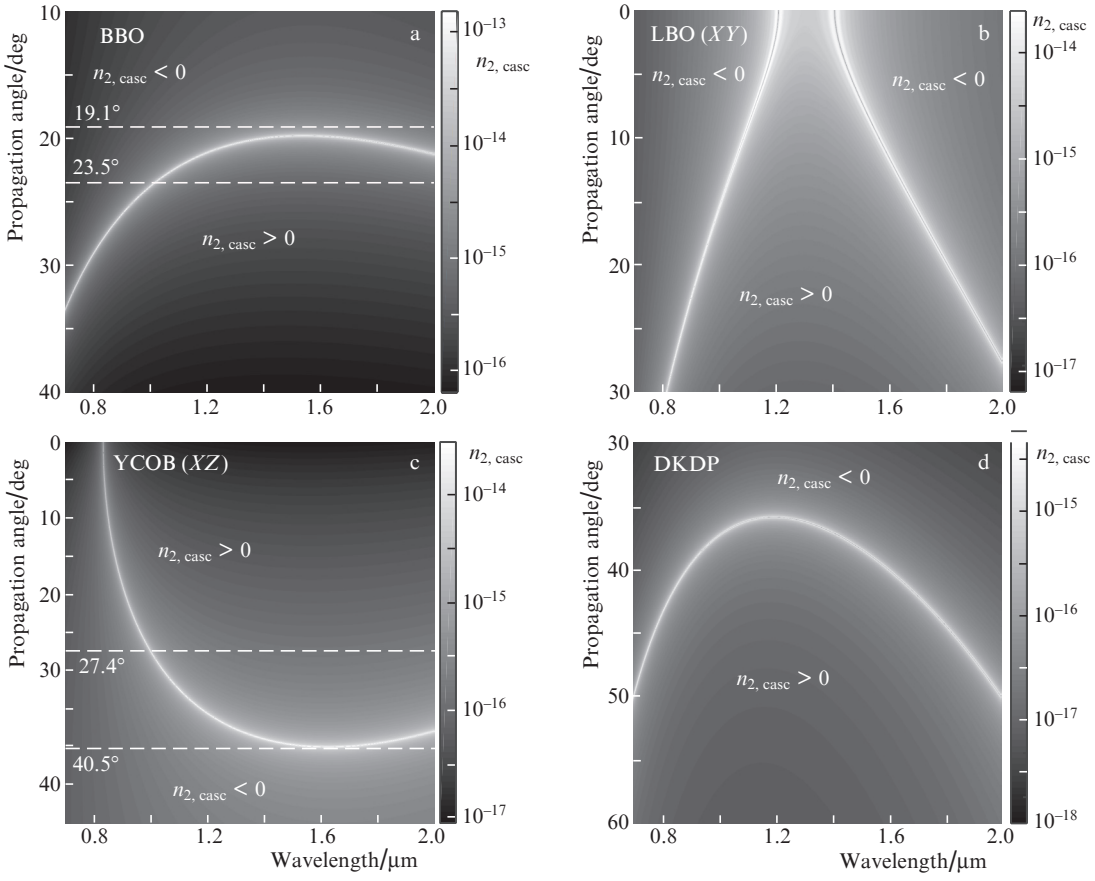

Figure 1. Spectral-angular dependences on the logarithmic scale of the effective cubic nonlinearity modulus $n_{2,\text{casc}}$ calculated using Eqn (2) for (a) BBO, (b) LBO (plane XY), (c) YCOB (XZ) and (d) DKDP crystals. The vertical axis shows the propagation angles of radiation relative to the Z axis for crystals BBO, YCOB and DKDP and to the X axis for LBO.

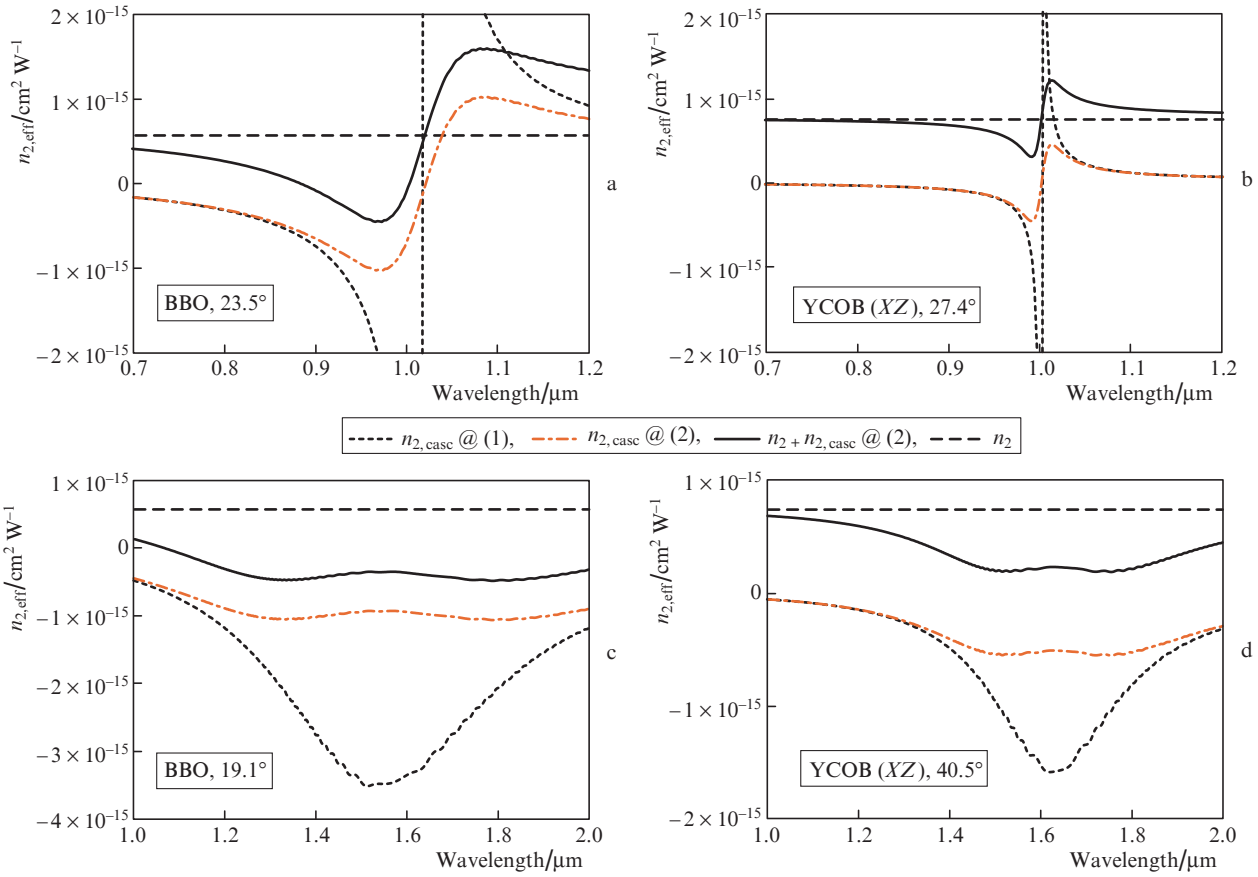

Figure 2. Spectral dependences of the effective cubic nonlinearity calculated using Eqns (1) and (2) at an intensity of 200 GW cm^{-2}, as well as the total effective nonlinearity for various crystals: (a) BBO at a propagation angle of 23.5°, (b) YCOB (*XZ* plane) at an angle of 27.4°, (c) BBO at an angle of 19.1° and (d) YCOB (*XZ*) at an angle of 40.5°.

high-efficiency conversion (all data are given at a peak intensity of 200 GW cm^{-2}). It is important to note that near the nonlinearity transition through zero, Eqn (2) can give a significant error.

The calculated profiles of effective cubic nonlinearity in the region of 0.83 μm are characterised by strong dispersion, which reduces the potential spectral width of the pulse transmitted through the crystal. The total effective cubic nonlinearity for BBO is negative, while in the case of YCOB it is positive for the chosen intensity.

The spectral region of 1.55–1.6 μm seems to be the most promising for the application of the proposed technique for broadening the spectrum of pulses in BBO and YCOB crystals. In this region, the intensity dependence of nonlinearity is retained, but the spectral dispersion becomes weak, the value of nonlinearity itself is noticeably negative and exceeds the Kerr cubic nonlinearity in absolute value.

3. Phase-compensated spectrum broadening in media with an alternating sign of effective cubic nonlinearity

3.1. Numerical modelling technique

Formulae (1) and (2) are not valid for any intensity and wave mismatch; moreover, they do not take into account the effect of group velocity dispersion, which is important when generating few-cycle pulses. Obviously, for complete description of the quadratic nonlinearity cascade effects, a numerical simulation of the SHG process is necessary. In the present work, it is based on the system of equations:

$$\frac{\mathrm{d}E_{1,k\omega}}{\mathrm{d}z} = \mathrm{i}(k_{1z} - k_{1,0})E_{1,k\omega} - \mathrm{i}\frac{\omega_1}{c}F_+ \times\left[\frac{\varepsilon_0 d_{\mathrm{eff}}}{n_{1,0}}E_1^* E_2 \exp(-\mathrm{i}\Delta k z) + \gamma_1\left(|E_1|^2 + \frac{2}{3}|E_2|^2\right)E_1\right],$$

$$\frac{\mathrm{d}E_{2,k\omega}}{\mathrm{d}z} = \mathrm{i}(k_{2z} - k_{2,0})E_{2,k\omega} - \mathrm{i}\frac{\omega_2}{c}F_+ \times\left[\frac{\varepsilon_0 d_{\mathrm{eff}}}{n_{1,0}}E_1^2 \exp(\mathrm{i}\Delta k z) + \gamma_2\left(|E_2|^2 + \frac{2}{3}|E_1|^2\right)E_2\right], \quad (3)$$

where $k_{mz} = k_{mz}(\omega, \theta(k_x)) = \sqrt{k_m^2(\omega, \theta(k_x)) - k_x^2 - k_y^2}$; $m = 1$, 2 (the first and the second harmonic, respectively); k_m is the wave vector; k_x and k_y are the projections of the wave vector on the X (critical to phase matching) and Y axes; $k_{m,0} = k_m(\omega_{m,0}, \theta_0)$; $\omega_{m,0}$ is the centre frequency; θ_0 is the phase-matching angle; $E_m = E_m(t, x, y)$ is the electric field in the coordinate–time domain; $E_{m,k\omega} = E_{m,k\omega}(\omega, k_x, k_y)$ is the electric field in the Fourier domain; F_+ is the direct Fourier transform; $\gamma_m = \varepsilon_0 n_{m,0} n_2/2$; n_2 is the coefficient of the Kerr cubic nonlinearity; $n_{m,0}$ is the refractive index; and $\Delta k = k_{2,0} - 2k_{1,0}$.

The system of equations (3) is derived from the unidirectional pulse propagation equation (UPPE) [16] by reducing the field equation to the equations for pulse envelopes with two carrier frequencies, the first harmonic and the second one [17]. The equation takes into account diffraction and beam drift due to birefringence. It can be used to describe pulses with a spectral width having the order of the central frequency. A specific feature of the application of this approach to modelling cascaded quadratic nonlinearity is the necessity of using a sufficiently small step, $dz \ll 2\pi/\Delta k$, due to the large value of Δk.

3.2. Spectral broadening in a BBO crystal near 0.83 μm

The results of modelling the spectrum broadening of a Gaussian pulse with 20 fs duration, a centre wavelength of 0.83 μm and a peak intensity of 200 GW cm^{-2} in a 10 mm-long BBO crystal are presented in Fig. 3 for two close propagation angles 23.5° and 25°. As already mentioned, the effective cubic nonlinearity in this case is negative, but it is characterised by strong dispersion, as a result of which, at a propagation angle of 23.5°, the spectra expand significantly, while at 25° the broadening is weaker and the spectrum is shifted to the IR region. Turning the nonlinearities on and off shows that the negative effective cubic nonlinearity leads to a narrowing of the spectrum and the main broadening is due to the Kerr cubic nonlinearity. Thus, in this case, it is not possible to implement the scheme with subsequent compensation for the nonlinear phase. However, as shown in Ref. [8], when using negative cascaded cubic nonlinearity in a BBO crystal in the spectral region of 1 μm, the considered scheme allows longer pulses to be compressed from 190 fs to about 30 fs.

3.3. Spectral broadening in a BBO crystal near 1.55 μm

For a pulse with the centre wavelength of 1.55 μm, duration of 20 fs, and intensity of 200 GW cm^{-2}, a 5-mm long BBO crystal with a propagation angle of 19.1° was chosen. At such a crystal length, the peak pulse intensity decreases by an order of magnitude due to dispersion spreading, after which its further increase does not lead to a noticeable broadening of the spectrum. For the propagation angle under consideration, as shown in Fig. 2c, at a sufficiently weak dispersion and large negative value of the effective cubic nonlinearity, there is a noticeable broadening of the spectrum with a small pulse duration increase. At the second stage, the pulse passes through a compensating NaCl crystal 20 mm long ($n_2 = 4.35 \times 10^{-16}$ cm^2 W^{-1}). This crystal was chosen because of the high group velocity dispersion in the considered spectral range (359 fs^2 cm^{-1} near 1.6 μm) to prevent the pulse spectrum from narrowing down due to the opposite sign of the effective cubic nonlinearity.

The simulation results for this case are presented in Fig. 4. A significant broadening of the spectrum is observed after the BBO crystal, and after the NaCl crystal, the spectrum is further smoothed (Fig. 4a). The duration of the transform-limited pulse at the output was about 7 fs, while the duration of the pulse compressed during phase compensation to the fourth order inclusive increased to 7.2 fs (the pulse profiles are shown in Fig. 4b), which corresponds to 1.5 cycles of the carrier frequency; the field profile is shown in Fig. 4c. The criterion for choosing the parameters of the spectral phase decomposition, and hence the chirped mirrors, was chosen to compensate for the nonlinear phase at a minimum pulse half-maximum width, the peak intensity being 200 GW cm^{-2}. We also note that, in contrast to pulse compression in media with Kerr cubic nonlinearity, in the case under consideration, there is an insignificant (within 1 fs) pulse shift, depending on the intensity (Figs 4d and 4e). Note that all calculations of the dependence of parameters on intensity were performed without taking the spatial profile of the pulse into account. Similar to the case of the Kerr cubic nonlinearity, a dependence of the duration of the compressed spectrally broadened pulse on the intensity is observed. The crystal length at the compensating stage was chosen so that the spatial dependence of the phase on the intensity was minimal (Fig. 4f). In this figure, the phase of the pulse is shown at the time corresponding to the maximum intensity of the pulse at the output of the crystals after the spectral phase compensation at the initial peak intensity of 200 GW cm^{-2}. For a NaCl crystal as long as 20 mm, the phase difference of the intensities, equal to 70% and 130% of the peak intensity, was about 0.1 rad. Losses of radiation power in the process of SHG were equal to 15%–20%.

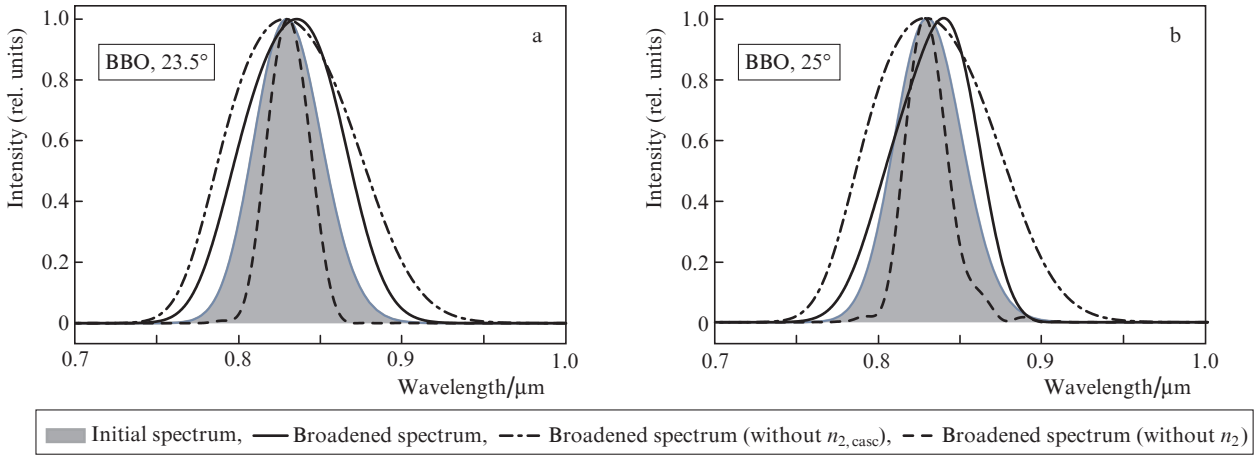

Figure 3. Pulse spectra before and after broadening; for analysis, the versions with the effective and Kerr cubic nonlinearities 'switched off' in BBO crystals are shown for the propagation angles of (a) 23.5° and (b) 25°.

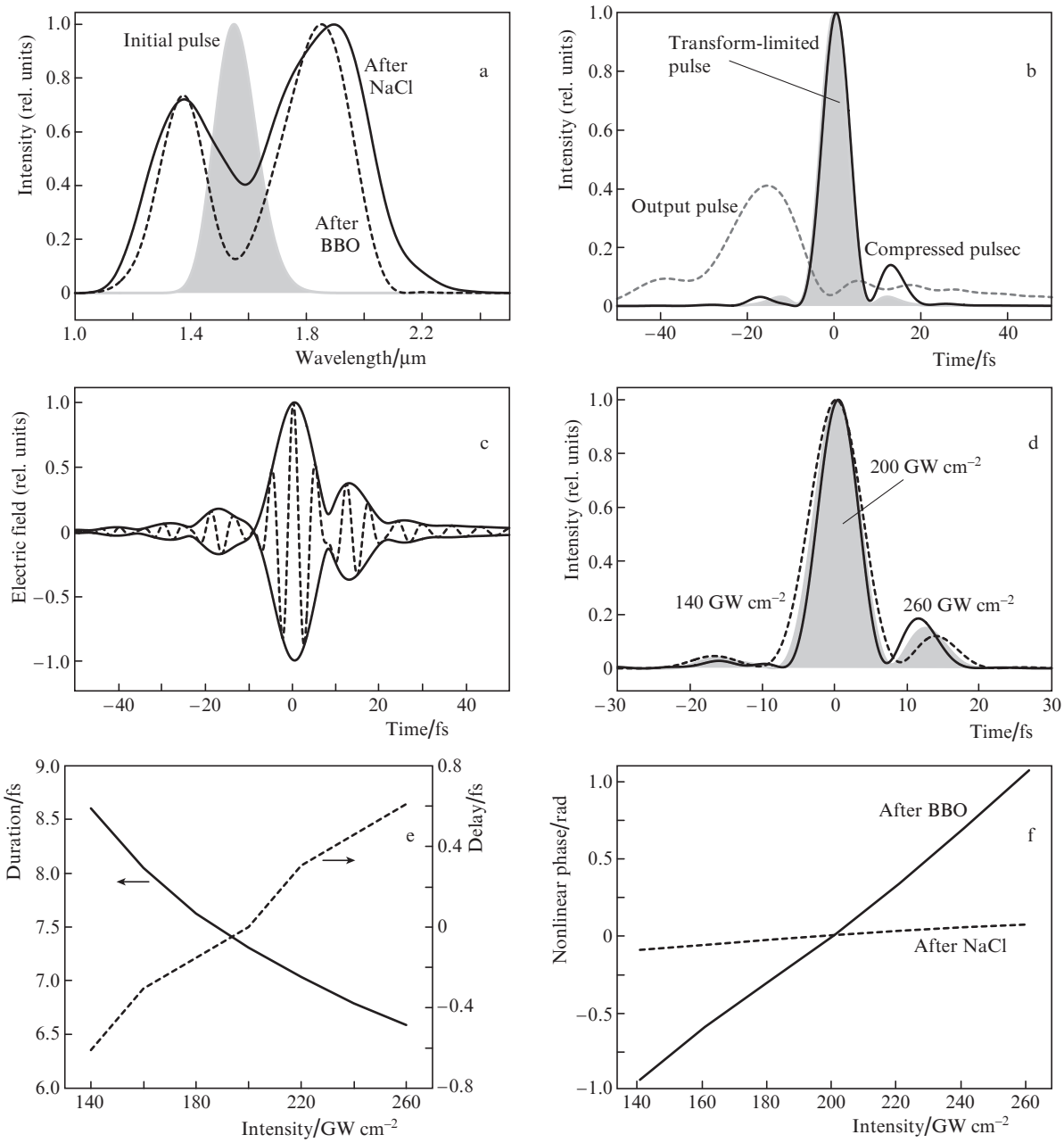

Figure 4. (a) Pulse spectra after broadening in a BBO crystal and subsequent phase compensation in a NaCl crystal; (b) temporal profiles of pulses at the output of NaCl crystal; (c) profile of the compressed pulse electric field; (d) intensity profiles of compressed pulses at various initial intensities; (e) duration of the compressed pulses and the relative time delay versus the initial intensity; (f) nonlinear phase versus the initial intensity at different stages of compression.

3.4. Beam focusability after compensated pulse compression

The best characteristic of the spatial nonlinear phase compensation quality is the focusability of compressed pulses. This property can be quantified by a change in the Strehl ratio, i.e., the ratio of the peak intensities of the focused radiation in the beams obtained without/with spatial phase compensation. Below we consider the focusing of the compressed pulses by a 90° parabolic mirror with the ratio $f/D = 0.5$ (f is the focal length and D is the beam diameter); the calculations were performed in the framework of the vector diffraction theory described in Ref. [18].

The initial intensity profile of the beam was generated as shown in Fig. 5, with amplitude inhomogeneities typical for high-power laser systems. As in previous calculations, the duration of the Gaussian pulse was 20 fs. In this case, the simulation was carried out taking into account the spatial effects described by Eqns (3), i.e., diffraction, birefringence, and self-focusing. Figure 6 shows the simulation results for the focusing of beams at different stages of compression. The beam profile after crystals and the spectral phase compensation is shown in Fig. 6a. For comparison of focusability, we used a pulse compressed after spectral broadening in a 6 mm-long quartz crystal to a duration of 7 fs; the spatial profile of the phase is shown in Fig. 6c. Modelling was carried out using Eqns (3) without terms describing the parametric interaction. In this case, the phase difference between the intensities of 70% and 130% of the peak intensity was 1.55 rad.

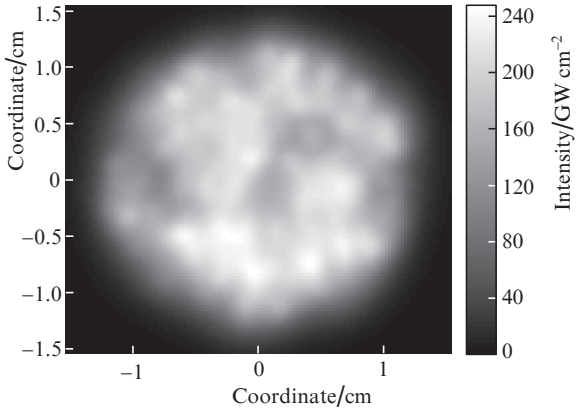

Figure 5. Initial spatial profile of the broadened pulse.

As follows from Fig. 6, the profile of the focused beam is symmetric in the case, when it has diffraction divergence (Fig. 6d), and when a nonlinear phase appears due to the Kerr (Fig. 6c) or cascaded quadratic nonlinearity after the compensation stage (Fig. 6b), the symmetry disappears. In the first case, the Strehl ratio (Str) was 0.535, and in the second case it was 0.897. Thus, the stage based on the NaCl crystal almost completely compensates for the spatial nonlinear phase. The spatial distribution of the beam phase is shown at the time corresponding to the maximum intensity I of the pulse at the crystals output after compensation of the spectral phase at the initial peak intensity of 200 GW cm^{-2}. In the same way, the phase was determined for calculating the Strehl ratio.

Figure 7 shows the dependences of the phase difference on the compensating crystal length L for the intensities of 160 and 240 GW cm^{-2}, as well as the Strehl ratio. The stage based on the NaCl crystal rapidly compensates for the spatial nonlinear phase: e.g., already at $L = 0.5$ cm, Str = 0.7, and at $L = 2$ cm it increases to 0.897. Both the pulse spreading due to

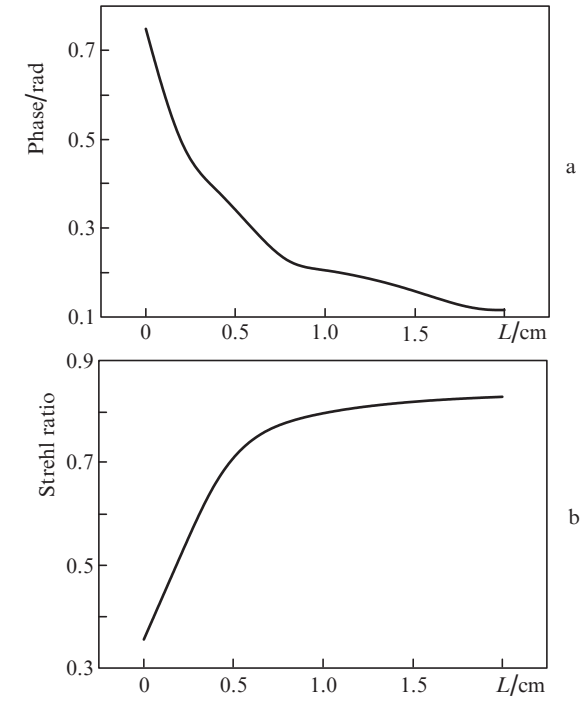

Figure 7. (a) Dependence of phase differences for intensities of 160 and 240 GW cm^{-2} on the length L of the NaCl crystal of the compensating stage and (b) Strehl ratio dependence on the length of the compensating NaCl crystal.

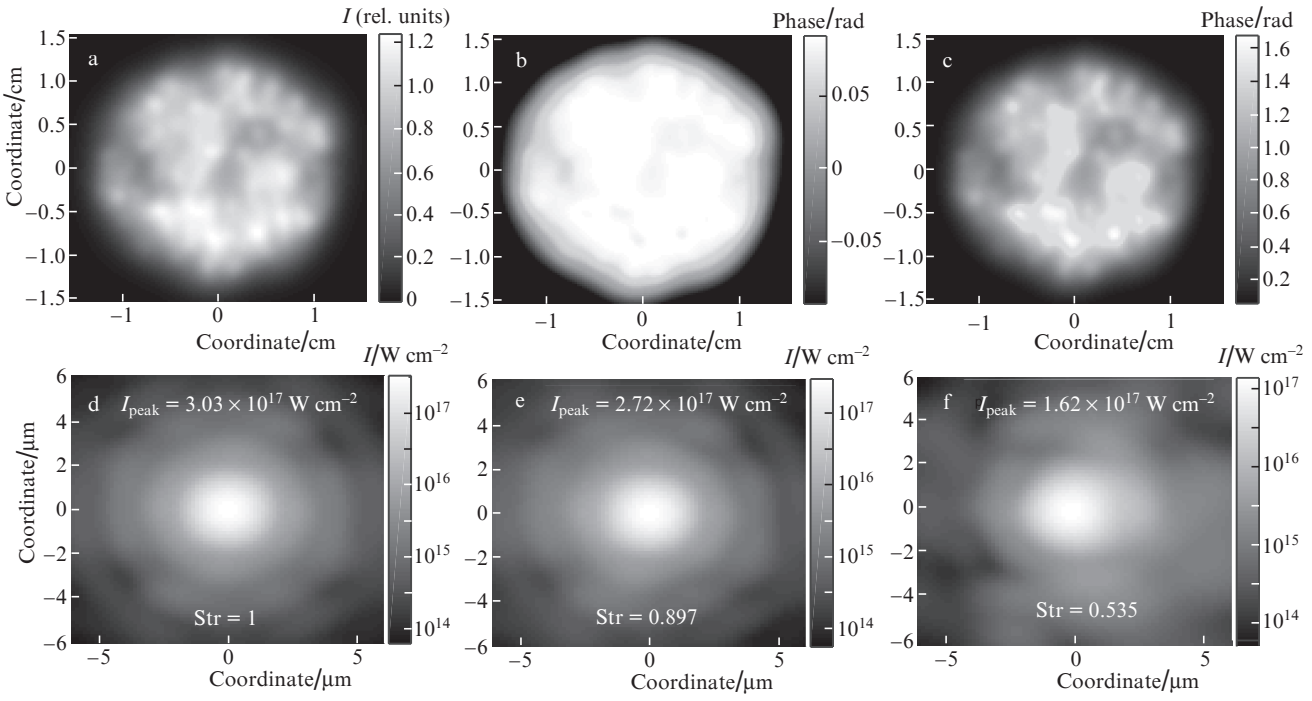

Figure 6. (a) Spatial profiles of the focused beam, (b) phase of the beam after broadening in BBO and compensation in NaCl, and (c) phase of the beam after broadening in quartz, as well as (d) profiles of the focused beam after broadening in quartz, (e) after broadening in BBO and compensation in NaCl with diffraction divergence, and (f) after broadening in BBO and compensation in NaCl.

dispersion and the more complex intensity dependence of the phase restrict the possibility of further, more complete, compensation of the nonlinear phase.

4. Conclusions

An original scheme of the temporal compression of femtosecond pulses in nonlinear media with different signs of effective cubic nonlinearity is proposed. It is shown that near 1.55 μm, the proposed scheme allows generating pulses with a duration of a few optical cycles (~7 fs) with a small value of the *B*-integral. In this case, according to the calculations, the Strehl ratio for a focused beam can reach 0.897, while for the scheme using a medium with Kerr nonlinearity (quartz crystal) it does not exceed 0.535. Thus, the proposed method allows improving the focusability of few-cycle pulses, reducing the level of spatial phase fluctuations caused by changes in intensity, and, thereby, facilitating the implementation of high-efficiency coherent summation of such pulses.

Acknowledgements. The work was supported by the Presidium of the Russian Academy of Sciences (Programme Extreme Light Fields and Their Interaction with Matter).

References

1. Mironov S.Yu., Ginzburg V.N., Lozhkarev V.V., Luchinin G.A., Kirsanov A.V., Yakovlev I.V., Khazanov E.A., Shaykin A.A. *Quantum Electron*., **41**, 963 (2011) [*Kvantovaya Elektron*., **41**, 963 (2011)].
2. Mourou G., Mironov S., Khazanov E., Sergeev A. *Eur. Phys. J. Spec. Top.*, **223**, 1181 (2014).
3. Tajima T., Mourou G., Wheeler J.A. *Laser Focus World*, **52**, 27 (2016).
4. Mironov S., Lassonde P., Kieffer J.C., Khazanov E., Mourou G. *Eur. Phys. J. Spec. Top*., **223**, 1175 (2014).
5. Lu C.H., Wu W.H., Kuo S.H., Guo J.Y., Chen M.C., Yang S.D., Kung A.H. *Opt. Express*, **27**, 15638 (2019).
6. Lu C.H., Witting T., Husakou A., Vrakking M.J., Kung A.H., Furch F.J. *Opt. Express*, **26**, 8941 (2018).
7. Hwang S.I., Park S.B., Mun J., Cho W., Nam C.H., Kim K.T. *Sci. Rep*., **9**, 1613 (2019).
8. Seidel M., Brons J., Arisholm G., Fritsch K., Pervak V., Pronin O. *Sci. Rep*., **7**, 1410 (2017).
9. Mironov S.Yu., Ginzburg V.N., Yakovlev I.V., Kochetkov A.A., Shaykin A.A., Khazanov E.A., Mourou G.A. *Quantum Electron*., **47**, 614 (2017) [*Kvantovaya Elektron*., **47**, 614 (2017)].
10. Mironov S.Yu., Khazanov E.A., Wheeler J., Gonin R., Mourou G., Dabu R., Cojocaru G., Ungureanu R., Serbanescu M., Banici R. *Quantum Electron*., **47**, 173 (2017) [*Kvantovaya Elektron*., **47**, 173 (2017)].
11. Ginzburg V.N., Yakovlev I.V., Zuyev A.S., Korobeynikova A.P., Kochetkov A.A., Kuz'min A.A., Mironov S.Yu., Shaykin A.A., Shaykin I.A., Khazanov E.A. *Quantum Electron*. **49**, 299 (2019) [*Kvantovaya Elektron*., **49**, 299 (2019)].
12. Farinella D.M., Wheeler J., Hussein A.E., Nees J., Stanfield M., Beier N., et al. *JOSA B*, **36**, A28 (2019).
13. Lu C.H., Tsou Y.J., Chen H.Y., Chen B.H., Cheng Y.C., Yang S.D., et al. *Optica*, **1**, 400 (2014).
14. DeSalvo R., Hagan D.J., Sheik-Bahae M., Stegeman G., Van Stryland E.W., Vanherzeele H. *Opt. Lett*., **17**, 28 (1992).
15. Saltiel S.M., in *Ultrafast Photonics – Proc. 56th Scottish Universities Summer School in Physics and NATO ASI* (St. Andrews, 2002).
16. Couairon A., Brambilla E., Corti T., Majus D., Ramírez-Góngora O.D.J., Kolesik M. *Eur. Phys. J. Spec. Top*., **199**, 5 (2011).
17. Bloembergen N. *Nonlinear Optics* (New York – Amsterdam: W.A. Benjamin, Inc., 1965; Moscow: Mir, 1966).
18. Varga P., Török P. *J. Opt. Soc. Am. A*, **17**, 2081 (2000).